



# Highly-stable tin-based perovskite nanocrystals produced by passivation and coating of gelatin

Bin Lyu<sup>a,c</sup>, Xu Guo<sup>a,c</sup>, Dangge Gao<sup>a,c,\*</sup>, Mengnan Kou<sup>a,c</sup>, Yajin Yu<sup>a,c</sup>, Jianzhong Ma<sup>a,c,\*\*</sup>, Shaowei Chen<sup>b</sup>, Hao Wang<sup>a,c</sup>, Ying Zhang<sup>a,c</sup>, Xin Bao<sup>a,c</sup>

<sup>a</sup> College of Bioresources Chemical and Materials Engineering, Shaanxi University of Science & Technology, Xi'an 710021, China

<sup>b</sup> Department of Chemistry and Biochemistry, University of California, 1156 High Street, Santa Cruz, CA 96064, USA

<sup>c</sup> National Demonstration Center for Experimental Light Chemistry Engineering Education (Shaanxi University of Science & Technology), Xi'an 710021, China

## ARTICLE INFO

### Keywords:

Tin-based perovskite nanocrystals  
Gelatin  
Passivation  
Coating  
Surface ligand  
Anti-mildew

## ABSTRACT

Lead-halide perovskite nanocrystals (NCs) are limited in commercial applications due to their high lead content. Developing lead-free perovskite NCs becomes a new choice. Among them, the tin-halide perovskite NCs exhibit the excellent photoelectric conversion efficiency, but has worse stability. Herein we describe an effective approach to the preparation of highly-stable all-inorganic tin-based perovskite NCs by using gelatin via interfacial passivation and coating, which leads to the retention of 77.46% of photoluminescence intensity even after the dispersion of the NCs in water for 3 d. The results show that gelatin form a "rich ligand" state on NC surface, such as amino-Sn, carboxylate-Sn and halogen-ammonium hydrogen-bonding interactions. The amino-Sn coordination would be replaced by carboxylate-Sn coordination when NCs are dispersed in polar-media. Meanwhile, gelatin is imparted excellent anti-mildew properties by NCs, which ensures long-lasting effect to NCs. This will promote the stability and sustainable development of the perovskite device.

## 1. Introduction

All-inorganic lead-halide perovskite nanocrystals (NCs) have been attracting widespread attention due to their low costs, narrow-band emissions, high photoluminescence quantum yields (QY) (Liu et al., 2017), and potential applications for light-emitting diodes, lasing, photovoltaics, etc (Zhang et al., 2016; Cha et al., 2016; Chen et al., 2018; Wang et al., 2017; Liu et al., 2017). However, conventional lead-halide perovskite NCs display a risk of lead contamination during production and/or disposal, where lead enrichment in the human body through the food chain can result in irreversible damages to human health. Thus the high lead level in these NCs remains a major factor limiting the commercial applications (Huang et al., 2016). Replacement of lead with non-toxic metals in the preparation of perovskite materials represents an ideal strategy for their commercialization (Leng et al., 2017). In fact, lead-free perovskite NCs, based on Bi(III), Sb(III), Ti(IV) and others, have indeed been prepared and displayed low toxicity (Xu et al., 2018). Among these, Sn(II)-halide perovskite NCs have been found to exhibit the excellent power conversion efficiency (Chen et al., 2019).

Nevertheless, traditional tin-halide perovskite NCs show poor stability and weak optical response, in comparison to the lead-halide counterparts. In addition, perovskite NCs are highly sensitive to the environment due to its strong ionicity (Meyns et al., 2016), unstable surface (Lin et al., 2016), and metastable structure (Zhang et al., 2014), and can even be rapidly dissolved by polar solvents to form large nanocrystals, resulting in structural collapse, shape transformation (Chen et al., 2016) and rapid decline of QYs (Li et al., 2017). In addition, Sn(II) can be easily oxidized to Sn(IV) in ambient condition, which leads to the formation of structural defects of halogen vacancies and interstitial metals, further exacerbating the collapse tendency of Sn(II)-based perovskite NCs (Fan et al., 2019). For instance, CsSnX<sub>3</sub> NCs was first reported in 2016, but with a low QY of only 0.14% (Jellicoe et al., 2016). Although the CsSnX<sub>3</sub> NCs were stable in colloidal solution for two weeks, the NCs would lose lots of photoluminescence due to the oxidation of Sn<sup>2+</sup> to Sn<sup>4+</sup> when exposed to air for only little time. Therefore, the stability and optical response of tin-halide perovskite NCs need to be markedly improved.

In the few studies of tin-halide perovskite NCs (Roo et al., 2016; Chen

\* Corresponding author at: College of Bioresources Chemical and Materials Engineering, Shaanxi University of Science & Technology, Xi'an 710021, China

\*\* Corresponding author at: College of Bioresources Chemical and Materials Engineering, Shaanxi University of Science & Technology, Xi'an 710021, China

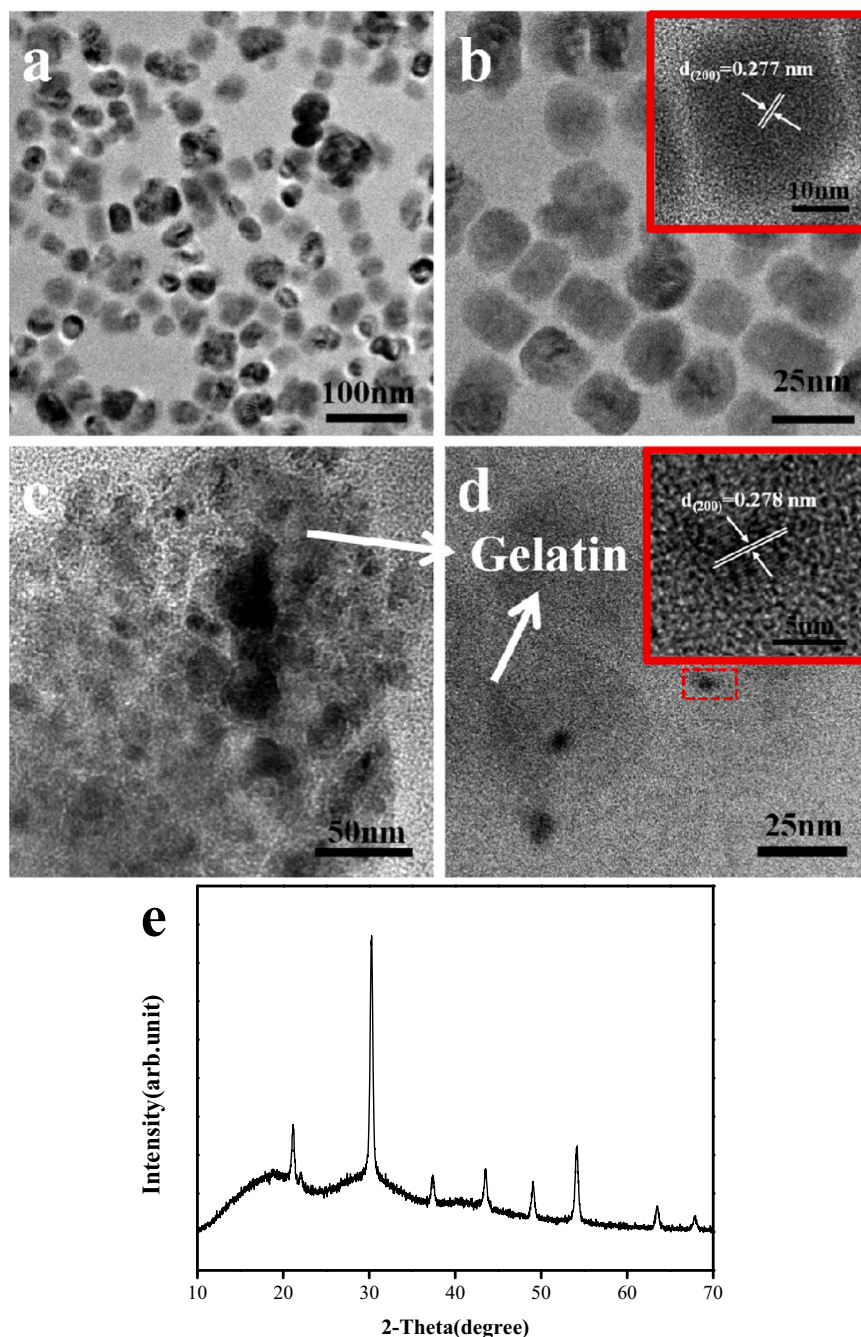
E-mail addresses: [dangge2000@163.com](mailto:dangge2000@163.com), [dangge2000@126.com](mailto:dangge2000@126.com) (D. Gao), [majz@sust.edu.cn](mailto:majz@sust.edu.cn) (J. Ma).

<https://doi.org/10.1016/j.jhazmat.2020.123967>

Received 24 March 2020; Received in revised form 11 September 2020; Accepted 11 September 2020

Available online 15 September 2020

0304-3894/© 2020 Elsevier B.V. All rights reserved.



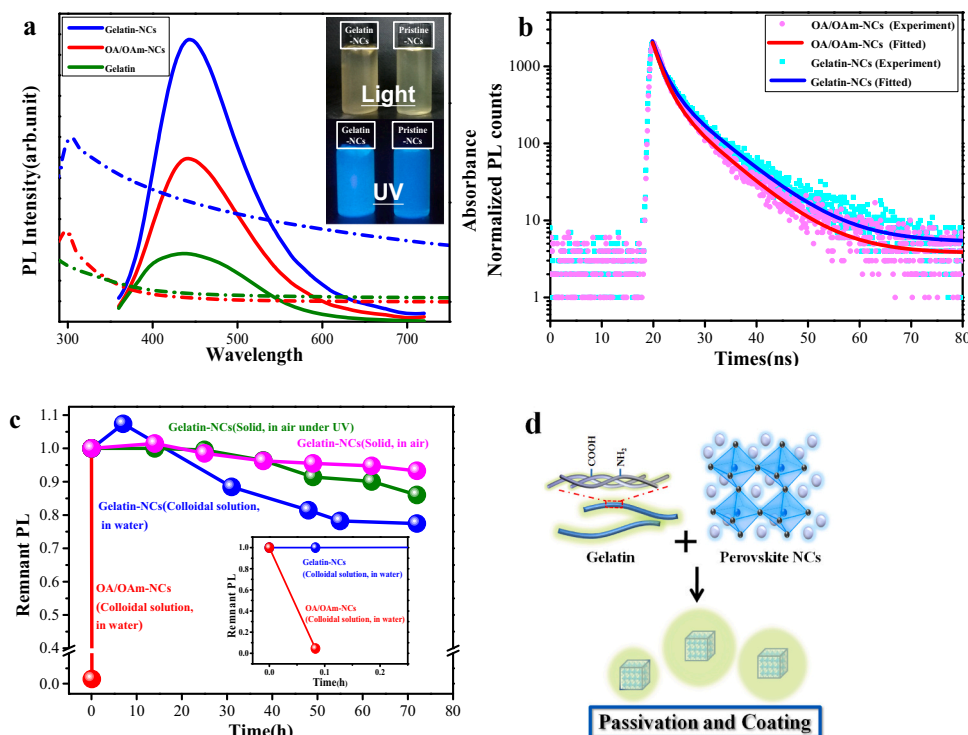
**Fig. 1.** TEM and XRD studies. (a, b) TEM images of OA/OAm-NCs. (c, d) TEM images of Gelatin-NCs. (e) XRD patterns of CsSnCl<sub>3</sub> decomposition products.

et al., 2016; Lin et al., 2019; Wang et al., 2017), perfluorooctanoic acid (PFOA) has been used to passivate the nanocrystals. For instance, for PFOA-stabilized CsSnBr<sub>3</sub> NCs, the interaction between F<sup>-</sup> and Sn<sup>2+</sup> and the steric hindrance of PFOA have been found to greatly improve the NC stability, leading to an increase of the PLQY to 2.1%. In fact, the optical response of the film underwent only a slight degradation (10%) under photoirradiation for 24 h (Wang et al., 2017). However, the high use of fluorine may have detrimental impacts on the environment. It will be highly desired to use biomass instead that is environmentally friendly and readily accessible.

Gelatin is the partial product of collagen hydrolysis, generally prepared from the skins and bones of animals, with abundant sources, good biocompatibility and degradability. More importantly, the long chain of gelatin has abundant carboxyl and amino groups which can be used to replace the oleic acid/oleylamine ligands for the surface passivation of

NCs, affording the NCs with much enhanced stability through multi-dentate chemistry. The antioxidant properties of gelatin also play an important role. Meanwhile, as not all perovskite structural defects are electronic in nature (Yang et al., 2019), the long molecular chains of gelatin can tightly coat the NCs and minimize erosion.

Herein, we demonstrate an effective strategy for the preparation of stable tin-based perovskite NCs by using biomass gelatin-capped CsSnCl<sub>3</sub> NCs as the illustrating example. The resulting gelatin-stabilized CsSnCl<sub>3</sub> NCs show a remarkable structural stability. Even after the NCs are dispersed in water for 72 h, 77.4% of the photoluminescence intensity can be retained. Spectroscopic studies confirm the NC surface passivation by gelatin due to the formation of stable carboxylate-Sn coordination and halogen-ammonium hydrogen-bonding. Remarkably, the gelatin-capped NCs also show high resistance to mildew, which enhances the durability of the gelatin passivation by



**Fig. 2.** Spectroscopic characterizations and Stability test of gelatin-NCs. (a) UV-vis absorption (dashed curves) and PL (solid curves) spectra of Gelatin-NCs, OA/OAm-NCs and gelatin. The excitation wavelength is set at 349 nm. Inset is the photographs of the gelatin-NCs and OA/OAm-NCs under the room light (above) and UV photoirradiation (= 365 nm) (below). (b) Time-resolved PL decay and fitting curves of gelatin-NCs and OA/OAm-NCs. (c) Relative PL values of OA/OAm-NCs and gelatin-NCs over time under different conditions (exposure to air, exposure to UV radiation and dispersion in water). Insert: remnant PL changes of OA/OAm-NCs and gelatin-NCs in 5 min (d) Schematic diagram of gelatin passivation and coating of NCs.

effectively reducing the risk of gelatin erosion caused by microorganisms such as mold.

## 2. Experimental section

### 2.1. Materials

Cs<sub>2</sub>CO<sub>3</sub>, SnCl<sub>2</sub>, cyclohexane, oleic acid (OA), oleylamine (OAm), and octadecene (ODE) were obtained from Shanghai Macklin Biochemicals Co., Ltd. Ethyl acetate were supplied by Tianjin Hongyan Chemical Reagents Co., Ltd. Glycerin and gelatin (Hydrolysate of animal skins, such as pigskin) were purchased from Tianjin Tianli Chemical Reagent Co., Ltd. and Tianjin Zhiyuan Chemical Reagent Co., Ltd., respectively. The above reagents were of analytical grade. All solvents were vacuum dried before use. All reagents were used as received without further purification.

### 2.2. Synthesis of CsSnCl<sub>3</sub> NCs

Cs-oleate was synthesized by reaction of Cs<sub>2</sub>CO<sub>3</sub> (0.35 mmol) with OA (0.5 mL) in octadecene (5 mL) and pre-heated to 120 °C before injection. SnCl<sub>2</sub> (0.133 mmol) and 5 mL ODE were loaded into a 3-neck flask, dried under vacuum at 100 °C for 1 h, then heated in an oil bath at 120 °C under a N<sub>2</sub> atmosphere for 1 h later and then mixed with OAm (0.5 mL) and OA (0.5 mL). The temperature was raised to 150 °C, and 0.4 mL of the Cs-oleate solution was swiftly injected for 5 s before the reaction was quenched by placing the mixture onto an ice-water bath.

### 2.3. Synthesis of gelatin-CsSnCl<sub>3</sub> NCs

Gelatin and glycerol at the mass ratio of 1:4 were added into a 100 mL 3-neck flask under stirring at 80 °C for 1 h until gelatin was completely dissolved. The OAm/OA-capped CsSnCl<sub>3</sub> NCs prepared above were then added into it under slightly stirring for 0.5 h in N<sub>2</sub> atmosphere. Finally, ethanol was added to the mixture to obtain a yellow precipitate, which was collected and further purified by a few cycle of centrifugation.

### 2.4. Mildew resistance test

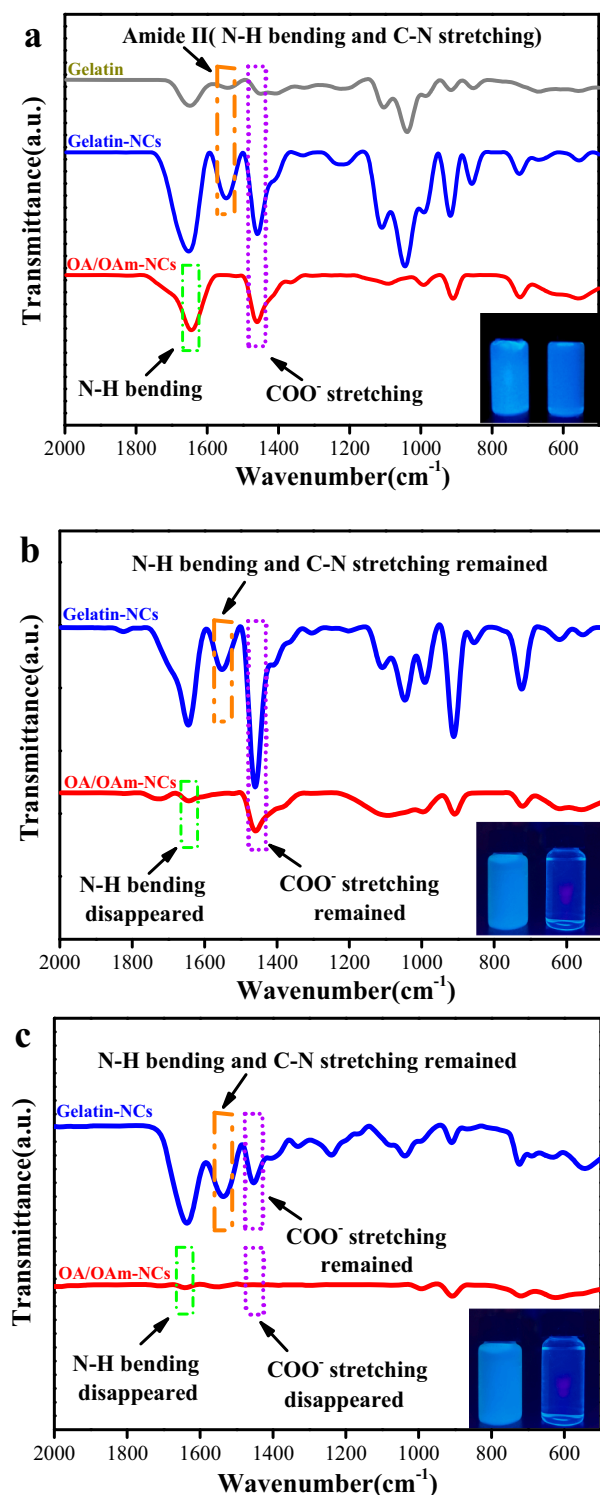
About 20 mL of a culture medium was poured into three sterilized dishes. Then injected 1 mL of PBS (phosphate buffer saline), gelatin aqueous solution and gelatin-NCs aqueous solution separately (to reach a same gelatin concentration). Last, the plates of culture medium were aseptically inoculated by spore suspensions (2–5 spores/drop) of aspergillus flavus at three places on the surface of the medium and incubated at 37 °C for 5 d.

### 2.5. Materials characterization

X-ray diffraction (XRD) patterns of the samples were acquired with the high-resolution diffractometer (D8 Advance, Bruker, Germany) with Cu K<sub>α</sub> radiation. Transmission electron microscopy (TEM, Hitachi, H-7650, Japan) was carried out to characterize the morphology of OA/OAm-NCs and gelatin-NCs. Photoluminescence measurements were conducted with an Edinburgh FS5 fluorescence spectrometer (United Kingdom). Fourier-transform infrared (FTIR) spectroscopic studies were performed with a Bruker Vector 22 infrared spectrometer (Germany). UV-vis spectra were obtained using an Agilent Cary 5000 spectrophotometers (United States). The surface charge of the samples was analyzed measured with a SZP06 Zeta potentiometer. X-ray photoelectron spectroscopy (XPS) studies were carried out with a Kratos AXIS SUPRA instrument (United Kingdom).

## 3. Results and discussion

Oleic acid/oleylamine (OA/OAm)-capped CsSnCl<sub>3</sub> NCs were first prepared by the hot injection method, and passivation of the NCs by gelatin was achieved by dispersing the NCs in glycerol with gelatin. The structures of the resulting OA/OAm-NCs were first examined by TEM measurements. Fig. 1a-b shows the representative TEM images of the OA/OAm-NCs, wherein the NCs can be found to exhibit a cubic structure with the lateral length about 18 nm. After gelatin passivation, the NC size was significantly reduced to ca. 7 nm (Fig. 1c-d). In addition, one can see that the gelatin-NCs exhibited clearly defined lattice fringes,



**Fig. 3.** Infrared spectra of gelatin-NCs and OA/OAm-NCs under different washing times (a) unwashed, (b) once, (c) three times. Insert: Photograph of the sample under UV light after different washing times, with gelatin-NCs on the left and OA/OAm-NCs on the right.

with an interplanar spacing of 0.278 nm (Fig. 1d) that can be assigned to the (2 0 0) plane of CsSnCl<sub>3</sub> (JCPDS No. 74-2058). During the experiment, we found that even the high-speed centrifugation purification process was very easy to cause the decomposition of CsSnCl<sub>3</sub> NCs, and the XRD characterization results in Fig. 1e confirmed that the precipitate was CsCl (JCPDS No. 05-0607), which was exactly consistent with

**Table 1**  
Stability parameter Comparisons of other related perovskites.

	Air stability	Photostability	Water Resistance	Reference
Gelatin-CsSnCl <sub>3</sub>	93.28% (72 h)	86.23% (72 h)	77.4%(72 h)	This work
PFOA-Hollow Cubic CsSnBr <sub>3</sub>		90% (24 h)		21
CsSn <sub>0.5</sub> Ge <sub>0.5</sub> I <sub>3</sub>	91% of the initial PCE (100 h)			10
BiOBr-Cs <sub>3</sub> Bi <sub>2</sub> Br <sub>9</sub>		80% (78 h)	90%(8 h)	8
Starch-MAPbI <sub>3</sub>			50% (more than 800 h stored in humid environment)	34

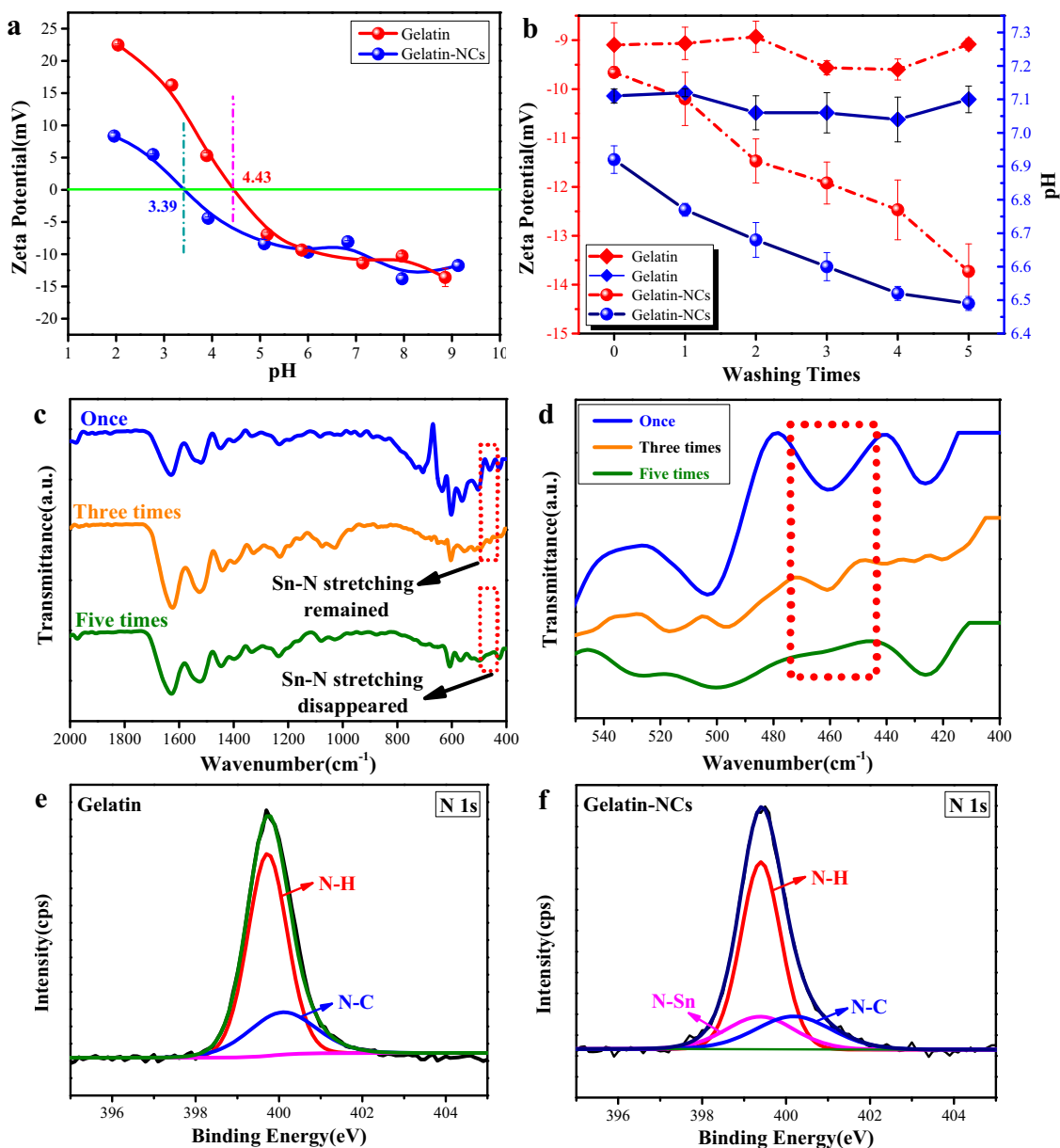
previous reports (Jellicoe et al., 2016). In fact, gelatin-NCs was dispersed in water and then characterized, which meant that there were strong interactions between NCs and gelatin, and gelatin effectively protected the NCs (Rao et al., 2018).

The optical properties of gelatin-NCs were then examined by UV-vis absorption and PL measurements. From Fig. 2a, one can see that photoluminescence intensity and UV-vis absorption of gelatin-NCs was significantly enhanced, wherein the UV-vis absorbance of gelatin-NCs was much higher than that of OA/OAm-NCs, causing the photoluminescence intensity increased by 72%. In addition, the full width at half-maximum (FWHM) was narrowed from 126 nm for the OA/OAm-NCs to 116 nm for the Gelatin-NCs. In order to avoid the interference of optically responsive substances, such as gelatin and precursor CsOA, we also evaluated the photoluminescence properties of these two materials at the excitation wavelength of 349 nm. The photoluminescence emission of the gelatin solution was only 30% of that for gelatin-NCs, while the emission of CsOA was less than 2% of that for gelatin-NCs under the same concentration. These suggested that the intense emission of gelatin-NCs was not simply caused by polymers or CsOA, but mainly due to the passivated NCs, where non-radiative transition by surface defects was effectively contained (Tang et al., 2018). This significant improvement in optical performance may be due to the abundant carboxyl and amino groups on the gelatin chain that bind to NCs, in comparison to the monodentate interaction of oleic acid/oleylamine ligands with NC surface. This "multi-point combination" formed the "rich ligand" state on the NC surface, and these active sites were all on the same gelatin molecular chain, so the possibility of ligand loss was greatly reduced. Moreover, there were many reactive groups in the gelatin molecular chain that can be combined.

The photophysical properties of the resulting gelatin-NCs were further studied by time-resolved photoluminescence measurements (Liu et al., 2017). Figure 2b shows the typical normalized photoluminescence decays for OA/OAm-NCs and gelatin-NCs at the excitation wavelength of 349 nm. The decay curves were fitted (Zhang et al., 2014):

$$R(t) = \sum A_i e^{-t/\tau_i}, i = 1, 2 \quad (1)$$

We can also clearly see that the photoluminescence of gelatin-NCs decayed slower than that of OA/OAm-NCs. The average recombination lifetime ( $\tau_{av}$ ) was estimated to be 7.33 ns for OA/OAm-NCs and 8.84 ns for gelatin-NCs. The overall lifetime of gelatin-NCs was increased by 20.57%, implying that gelatin-capping effectively suppressed the formation of nonradiative recombination pathways on the NC surface. It is well-known that photoluminescence lifetime of NCs was closely related to its extent of surface passivation (Cho et al., 2015; Xie et al., 2019), where incomplete surface passivation typically leads to the formation of surface defects and hence diminishment of photoluminescence lifetimes (Jaramillo-Quintero et al., 2015). Taken together, these results show that gelatin passivation effectively improves the NC



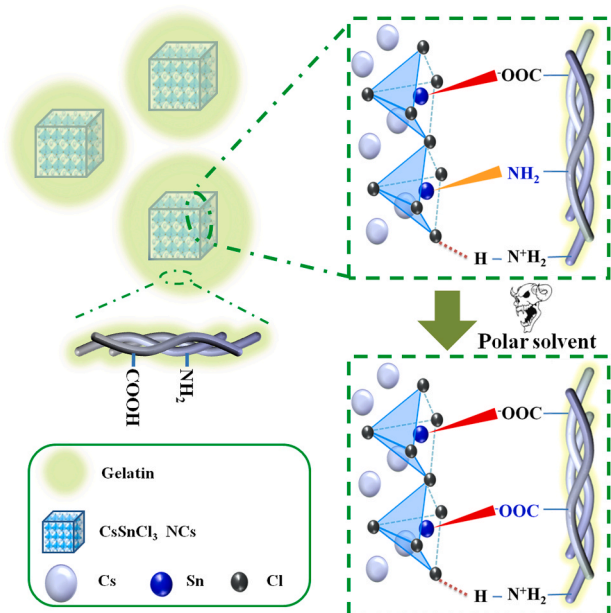
**Fig. 4.** (a) gelatin-NCs and gelatin isoelectric point, (b) Surface charge and pH changes of gelatin-NCs and gelatin aqueous solution as the times of washing increased, (c) Infrared spectrum of gelatin-NCs after different times of washing ( $2000\text{ cm}^{-1}$ – $400\text{ cm}^{-1}$ ), (d) is partial enlargement of (c), (e) XPS spectra of N 1s in gelatin, (f) XPS spectra of N 1s in Gelatin-NCs.

photoluminescence (Dang et al., 2017).

The stability of gelatin-NCs was then tested under extreme conditions. The gelatin-NCs solid was put into a vacuum oven to remove solutions or further dispersing the OA/OAm-NCs/gelatin-NCs in water, and then the samples were placed in different environments. For comparison, the same treatment was performed on the OA/OAm-NCs. From Fig. 2c, it can be seen that gelatin-NCs exhibited ultra-high stability under exposure to air, retaining as high as 93.28% (pink line) of the photoluminescence intensity after 72 h in the dark and 85% even after exposure to UV irradiation for 72 h (green line). In the relevant water resistance test, the photoluminescence response of OA/OAm-NCs suffered more than 95% loss within 5 min, likely because the addition of water to the NCs solution in cyclohexane caused delamination, which caused the loss of ligand to self-aggregation and photoluminescence quenching, even decompose. By contrast, the photoluminescence intensity of gelatin-NCs showed almost no change after 5 min (inset), and more than 75% photoluminescence intensity was retained after 72 h (blue line). The excellent stability of gelatin-

NCs was attributed to the passivation and encapsulation of NCs by gelatin, as shown in Fig. 2d. Gelatin played an important role in resisting water attack, as the hygroscopic nature of the gelatin network stabilized and protected the perovskite from water (Giuri et al., 2018). The large number of hydrophilic groups on gelatin were consumed due to binding to the surface of NCs, which also greatly reduced the solubility of gelatin-NCs. And the large molecular weight gelatin tightly coated and isolated the NCs, which greatly reduced self-aggregation and oxidation of NCs (Jaramillo-Quintero et al., 2015). In addition, it has been known that excessive moisture caused the gelatin fiber to swell by three to five times, further reducing the porosity between fibers and preventing moisture intrusion.

Carboxylate can be coordinated with the metal element at the B site in the perovskite structure, and alkylammonium interacts with the halogen through hydrogen bond (Pan et al., 2018). Such organic ligand adsorption on the NC surface is dynamically balanced. For OA/OAm-NCs, in order to balance the charge, protonated oleylamine would carry away halogen or oleic acid when leaving the NC surface. The loss of ligands on the NC



**Scheme 1.** Schematic of gelatin-NCs with excellent polar solvents stability.

surface was one of the main reasons for the instability of NCs. To some extent, the presence of NCs surface ligands after washing by organic solvents reflects the stability of NCs (Wei et al., 2018; Brown et al., 2014). Thus, the gelatin-NCs and OA/OAm-NCs samples were washed by polar solvents. The structures before and after washing were then characterized and compared by FTIR measurements. From Fig. 3a, one can clearly see the C-N stretching vibration and N-H bending vibration at  $1541\text{ cm}^{-1}$  for Amima II of gelatin and gelatin-NCs, the N-H bending vibration at  $1645\text{ cm}^{-1}$  for Oleamine of OA/OAm-NCs, and the characteristic carboxylate symmetrical stretching vibration at  $1450\text{ cm}^{-1}$  both for OA/OAm-NCs and gelatin-NCs. After one wash with organic solvents, the N-H bending vibration of OA/OAm-NCs vanished, along with an almost complete disappearance of photoluminescence. When the washing was repeated three times, the characteristic carboxylate stretching vibration peak of OA/OAm-NCs also disappeared, along with a further decrease of the photoluminescence. By contrast, these vibrational peaks remained very visible with gelatin-NCs, and the photoluminescence intensity was almost unchanged.

The vanishment of the photoluminescence of OA/OAm-NCs after solvent washing may be ascribed to polar solvent-induced ligand and ion migration on the NC surface, "surface dissolution" and "recrystallization" (Roo et al., 2016; Pan et al., 2018; Wei et al., 2018; Brown et al., 2014). Eventually, the NCs were dissolved into larger nanocrystals, even decompose, causing the optical response of NCs to drop sharply. This also confirmed that the NCs prepared in the oleic acid/oleylamine system were extremely unstable. It is worth noting that the N-H bending vibration peak of OA/OAm NCs disappeared, while the characteristic carboxylate stretching vibration peak remained, which indicated that the oleic amine ligands on the NC surface had been completely lost, while oleic acid ligands remained. In other words, the binding of amino groups to NCs was weaker than that of carboxyl groups, consistent with results from previous reports (Pan et al., 2018). On the contrary, the Amima II and carboxylate stretching vibration peak of gelatin-NCs remained clearly defined, indicating that the ligands on the NC surface were hardly lost and had high resistance to solvent washing.

After solvent washing for three times, it can be seen from Fig. 3c that the N-H bending vibration and carboxylate stretching vibration were not observed with OA/OAm-NCs and no photoluminescence under UV light irradiation, which meant that oleic acid ligands were also completely removed. Yet, the Amima II and carboxylate stretching vibrations of gelatin-NCs were still clearly visible. This indicates a stable ligand shell

of gelatin-NCs and hence its high stability, likely a result of multidendate interactions with NCs. Although the ligands on the surface of NCs were in the process of dynamic equilibrium, it was almost impossible to simultaneously migrate all the ligands of gelatin and NCs, not to mention the numerous "alternative ligands" on the surface of gelatin.



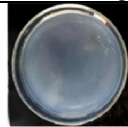

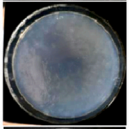
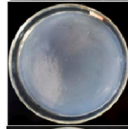

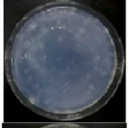
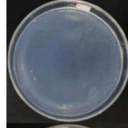
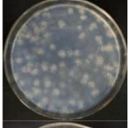
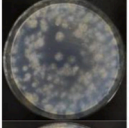
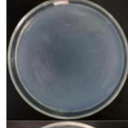
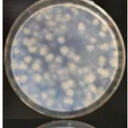
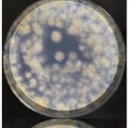

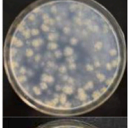
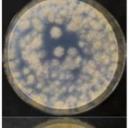
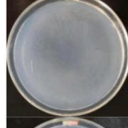
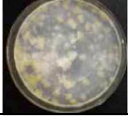

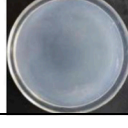
The stability of Sn-, Bi-perovskite materials, Pb-based perovskite materials stabilized by biomass materials is summarized in Table 1. The gelatin-NCs prepared above can be seen to show high stability, especially in terms of water resistance. Water and oxygen have been known to show great influence on Sn-based perovskite NCs (Chen et al., 2016). The oxygen barrier and excellent water resistance exhibited by gelatin is important for greatly improving the stability of tin-based perovskite NCs. This is likely due to multiple active groups of gelatin that can interact with NCs, such as the carboxyl groups that form coordination bonds with the central metal centers, and the amino groups that form hydrogen bond with the halogen, leading to strong binding of ligands to the NC surface, the oxidation resistance of gelatin also plays an important role.

Gelatin is an amphoteric polymer. Studying the change of its isoelectric point (pI) is beneficial to study the change of its internal bonding mode. The pI of gelatin-NCs was estimated to be 3.39, a significant drop as compared to that (4.43) of gelatin alone (Fig. 4a). Prior to solvent washing, the pH of gelatin-NCs was 6.92, which was lower than 7.11 of gelatin (Fig. 4b). This implies that the degree of carboxyl dissociation was significant increased in gelatin-NCs. From Fig. 4b, one can see that with an increasing number of washing cycles, the pH and surface charge of the gelatin aqueous solution remained virtually unchanged, where a significant decrease can be seen with gelatin-NCs. This suggests that during the washing process, carboxyl groups of the gelatin were further ionized and bound on NCs, resulting in a decrease of the solution pH and the surface charge of the gelatin-NCs. Infrared characterization (Fig. 4c-d) provided a basis for explaining this phenomenon, which shows a medium-intensity peak at  $460\text{ cm}^{-1}$  (Yin et al., 2004). That is, in the gelatin-NCs system, carboxylate and amino groups both coordinate with Sn. the Sn-N stretching vibration became gradually weakened as the washing times increased, and after five washing cycles, the N-Sn stretching vibration peak almost vanished. Consistent results were obtained in XPS measurements. the N1s spectrum can be deconvoluted into two peaks of N-C (400.1 eV) and N-H (399.7 eV), which correspond to the peptide bond and amino group in gelatin, respectively (Fig. 4e). From Fig. 4f, the N1s spectrum can be deconvoluted into three peaks, in addition to the N-C and N-H species, a new species appeared, which was ascribed to N-Sn. Note that the fraction of protonated amino groups increases significantly in gelatin-NCs, thus the relative fraction of N-H bond increased and that of N-C bond decreased. However, in the N1s spectrum of gelatin-NCs, the fraction of N-H bond decreased and a new peak appeared, which meant that some N-H bonds were involved in the formation of N-Sn bonds. These results indicated that there were not only  $[\text{Cl}\cdots\text{H}-\text{N}^+]$  hydrogen-bonding and carboxylate-Sn coordination interactions on the surface of NCs, but also N-Sn coordination.

Based on the above results, the interaction mechanism of gelatin and  $\text{CsSnCl}_3$  NCs is proposed and illustrated in Scheme 1. The carboxylate and amino groups on the gelatin coordinate with Sn in NCs, and the protonated amino groups are bonded to the halogen through hydrogen-bonding. The rich functional groups of gelatin occupy the active sites on the NC surface, forming a "rich ligand" state that is difficult to lose in the normal condition. Therefore, when gelatin fully passivated the NC surface, it effectively suppressed the formation of surface defects. Meanwhile, the coating of NCs by gelatin prevented environmental erosion and self-agglomeration between NCs. When gelatin-NCs was attacked by polar solvents, the carboxylate-Sn on gelatin-NCs would replace the weaker amino-Sn. enhancing the NC stability. Thereby ionization of the carboxyl group on the gelatin-NCs was further increased, reducing the system charge and pH.

As a biomass material, gelatin has been known to be easily attacked by mold during use, which may lose the ability to passivate and coat NCs. In order to further verify the reliability of gelatin-NCs, we

**Table 2**  
Test of gelatin-NCs anti-mildew performance.

Time	(a) 1 mL PBS+ 1 mL bacterial suspension	(b) 1 mL Gelatin solution+ 1 mL bacterial suspension	(c) 1 mL Gelatin-NCs solution+ 1 mL bacterial suspension
0 h			
32 h			
40 h			
48 h			
56 h			
72 h			
120 h			

conducted a mildew test of gelatin-NCs by common molds (*Aspergillus flavus*), since gelatin-NCs had been proven to show good stability in water and air. Experimentally, gelatin-NCs were exposed to water and air during the entire mold-proof study. Table 2 shows the photographs of aqueous solutions of (a) PBS (phosphate buffer saline), (b) gelatin, and (c) gelatin-NCs in the presence of the bacteria for up to 120 h. One can see that the mold in column b was more prosperous than column a, because gelatin was a nutrient rich in nitrogen and carbon sources for mold, which greatly promoted the growth of mold. On the contrary, there was no mold growth in column c even after 120 h's culture time. This strong anti-mildew properties of gelatin-NCs was likely due to the following: when NCs were exposed to light, the absorption of photons by NCs led to transfer of electrons from the valence band (VB) to the conduction band (CB), leaving holes on VB. After light excitation, electron transitioned to the LUMO state of CB, while hole migrated to the homomorphism of VB. In addition, trapping electrons in CB can produce  $O_2^{\cdot-}$  as the redox potentials of  $H_2O(OH^{\cdot})/\cdot OH$  and  $O_2/\cdot O_2^{\cdot-}$  were located within the band gap of  $CsSnCl_3$  NCs.  $O_2^{\cdot-}$  and  $\cdot OH$  radicals were highly active antibacterial reagents, which greatly increased the anti-mildew property of the sample (Paul et al., 2019; Pu et al., 2017). This anti-mildew performance played an important role in the long-term function of gelatin and eliminates the risk of microbe attack of the substrate in practical applications.

#### 4. Conclusions

In summary, this study demonstrates that abundant green natural biomass materials gelatin can be used as the passivating reagent for tin-

based perovskite NCs, which not only reduce environmental pollution and but also enhance the performance of the tin-based perovskite NCs. Experimentally, stable Sn-based perovskite NCs were produced by passivation with gelatin, a biomass macromolecular material. The optical response of gelatin-NCs was found to be significantly improved, in which the photoluminescence intensity increased by 72%, as compared to the conventional OAm/OA-NCs. The gelatin-NCs also exhibited markedly improved stability, where 77.4% of the emission was retained after dispersion in water for 3 d. This is because in polar solvents, carboxylate-Sn coordination and halogen-ammonium hydrogen-bonding between NCs and gelatin remained largely intact, and the weaker amino-Sn coordination was replaced by the stronger carboxylate-Sn coordination. The anti-mildew property of gelatin can also enhance the scope of applications of perovskite NCs.

#### Acknowledgements

This work is supported financially by the Program of National Natural Science Foundation of China (21878182), Science Foundation for Distinguished Young Scholars of Shaanxi Natural Science Basic Research Program (S2020-JC-JQ-0114) and High-level Talents Special Support Plan Youth Talents Project of Shaanxi Province.

#### CRediT authorship contribution statement

Dangee Gao had the idea for and designed the experiments. Bin Lyu, Dangee Gao and Jianzhong Ma supervised the work. Xu Guo and Mengnan Kou performed the fabrication, characterization and mildew test of

gelatin-NCs and OA/OAm-NCs with the assistance of Yajin Yu, Ying Zhang, and Xin Bao. Xu Guo wrote the first draft of the manuscript and Bin Lyu, Dangee Gao, Jianzhong Ma and Shaowei Chen provided major revision. All authors discussed the results and commented on the manuscript.

## Declaration of Competing Interest

The authors declare no competing financial interest.

## Author contributions

D.G. had the idea for and designed the experiments. B.L., D.G. and J. M. supervised the work. X.G. and M.K. performed the fabrication, characterization and mildew test of gelatin-NCs and OA/OAm-NCs with the assistance of Y.Y., Y.Z., X.B. and H.W., X.G. wrote the first draft of the manuscript and B.L., D.G., J. M. and S.C. provided major revision. All authors discussed the results and commented on the manuscript.

## References

- Brown, P.R., Kim, D., Lunt, R.R., Zhao, N., Bawendi, M.G., Grossman, J.C., Bulović, V., 2014. Energy level modification in lead sulfide quantum dot thin films through ligand exchange. *ACS Nano* 8, 5863–5872. <https://doi.org/10.1021/nm500897c>.
- Cha, M., Da, P., Wang, J., Wang, W., Chen, Z., Xiu, F., Zheng, G., Wang, Z.S., 2016. Enhancing perovskite solar cell performance by interface engineering using CH<sub>3</sub>NH<sub>3</sub>PbBr<sub>0.9</sub>I<sub>0.1</sub> quantum dots. *Am. Chem. Soc.* 138, 8581–8587. <https://doi.org/10.1021/jacs.6b04519>.
- Chen, L., Dai, J., Lin, J., Mo, T., Lin, H., Yeh, H., Chuang, Y., Jiang, S.A., Lee, C.R., 2018. Wavelength-tunable and highly stable perovskite-quantum-dot-doped lasers with liquid crystal lasing cavities. *ACS Appl. Mater. Interfaces* 10, 33307–33315. <https://doi.org/10.1021/acsami.8b08474>.
- Chen, M., Ju, M.G., Garces, H.F., Carl, A.D., Ono, L.K., Hawash, Z., Zhang, Y., Shen, T., Qi, Y., Grimm, R.L., Pacifici, D., Zeng, X.C., Zhou, Y., Padture, N.P., 2019. Highly stable and efficient all-inorganic lead-free perovskite solar cells with native-oxide passivation. *Nat. Commun.* 10, 1–8. <https://doi.org/10.1038/s41467-018-07951-y>.
- Chen, L.J., Lee, C.R., Chuang, Y.J., Wu, Z.H., Chen, C., 2016. Synthesis and optical properties of lead-free cesium tin halide perovskite quantum rods with high-performance solar cell application. *Phys. Chem. Lett.* 7, 5028–5035. <https://doi.org/10.1021/acs.jpclett.6b02344>.
- Chen, J., Liu, D., AL-Marri, M., Nuutila, L., Lehtivuori, H., Zheng, K., 2016. Photostability of CsPbBr<sub>3</sub> perovskite quantum dots for optoelectronic application. *Sci. China Mater.* 59, 719–727. <https://doi.org/10.1007/s40843-016-5123-1>.
- Cho, H., Jeong, S.H., Park, M.H., Kim, Y.H., Wolf, C., Lee, C.L., Heo, J.H., Sadhanala, A., Myoung, N., Yoo, S., Im, S.H., Friend, R.H., Lee, T.W., 2015. Overcoming the electroluminescence efficiency limitations of perovskite light-emitting diodes. *Science* 350, 1222–1225. <https://doi.org/10.1126/science.aad1818>.
- Dang, Z., Shamsi, J., Akkerman, Q., Imran, M., Bertoni, G., Brescia, R.P., 2017. Low-temperature electron beam-induced transformations of cesium lead halide perovskite nanocrystals. *ACS Omega* 2, 5660–5665. <https://doi.org/10.1021/acsomega.7b01009>.
- Fan, Q., Biesold-McGee, G.V., Xu, Q., Pan, S., Peng, J., Ma, J., Lin, Z., 2019. Lead-free halide perovskite nanocrystals: crystal structures, synthesis, stabilities, and optical properties. *Angew. Chem. Int. Ed.* 59, 1030–1046. <https://doi.org/10.1002/ange.201904862>.
- Giuri, A., Masi, S., Listort, A., Gigli, G., Colella, S., Corcione, C.E., Rizzo, A., 2018. Polymeric rheology modifier allows single-step coating of perovskite ink for highly efficient and stable solar cells. *Nano Energy* 54, 400–408. <https://doi.org/10.1016/j.nanoen.2018.10.039>.
- Huang, S., Li, Z., Kong, L., Zhu, N., Shan, A., Li, L., 2016. Enhancing the stability of CH<sub>3</sub>NH<sub>3</sub>PbBr<sub>3</sub> quantum qots by embedding in silica spheres derived from tetramethyl orthosilicate in “waterless” toluene. *J. Am. Chem. Soc.* 138, 5749–5752. <https://doi.org/10.1021/jacs.5b13101>.
- Jaramillo-Quintero, O.A., Sanchez, R.S., Rincon, M., Mora-Sero, I., 2015. Bright visible-Infrared light emitting diodes based on hybrid halide perovskite with Spiro-OMeTAD as a hole-injecting layer. *J. Phys. Chem. Lett.* 6, 1889–1890. <https://doi.org/10.1021/acs.jpcclett.5b00732>.
- Jellicoe, T.C., Richter, J.M., Glass, H.F., Tabachnyk, M., Brady, R., Dutton, S.E., Rao, A., Friend, R.H., Credgington, D., Greenham, N.C., Böhm, M.L., 2016. Synthesis and optical properties of lead-free cesium tin halide perovskite nanocrystals. *J. Am. Chem. Soc.* 138, 2941–2944. <https://doi.org/10.1021/jacs.5b13470>.
- Leng, M., Yang, Y., Zeng, K., Chen, Z., Tan, Z., Li, S., Li, J., Xu, B., Li, D., Hautzinger, M. P., Fu, Y., Zhai, T., Xu, L., Niu, G., Jin, S., Tang, J., 2017. All-inorganic bismuth-based perovskite quantum qots with bright blue photoluminescence and excellent stability. *Adv. Funct. Mater.* 28 (1), 1704446 <https://doi.org/10.1002/adfm.201704446>.
- Lin, J., Gomez, L., Weerd, C. de, Fujiwara, Y., Gregorkiewicz, T., Suenaga, K., 2016. Direct observation of band structure modification nanocrystals of CsPbBr<sub>3</sub> perovskite. *Nano Lett.* 16, 7198–7202. <https://doi.org/10.1021/acs.nanolett.6b03552>.
- Lin, J.T., Liao, C.C., Hsu, C.S., Chen, D.G., Chen, H.M., Tsai, M.K., Chou, P.T., Chiu, C.W., 2019. Harnessing dielectric confinement on tin perovskites to achieve emission quantum yield up to 21%. *J. Am. Chem. Soc.* 141, 10324–10330. <https://doi.org/10.1021/jacs.9b03148>.
- Liu, F., Ding, C., Zhang, Y., Ripolles, T.S., Kamisaka, T., Toyoda, T., Hayase, S., Minemoto, T., Yoshino, K., Dai, S., Yanagida, M., Noguchi, H., Shen, Q., 2017. Colloidal synthesis of air-stable alloyed CsSn<sub>1-x</sub>Pb<sub>x</sub>I<sub>3</sub> perovskite nanocrystals for use in solar cells. *J. Am. Chem. Soc.* 139, 16708–16719. <https://doi.org/10.1021/jacs.7b08628>.
- Liu, H., Wu, Z., Shao, J., Yao, D., Gao, H., Liu, Y., Yu, W., Zhang, H., Yang, B., 2017. CsPb<sub>x</sub>Mn<sub>1-x</sub>Cl<sub>3</sub> perovskite quantum qots with high Mn substitution ratio. *ACS Nano* 11, 2239–2247. <https://doi.org/10.1021/acsnano.6b08747>.
- Liu, F., Zhang, Y., Ding, C., Kobayashi, S., Shen, Q., 2017. Highly luminescent phase-stable CsPbI<sub>3</sub> perovskite quantum dots achieving near 100% absolute photoluminescence quantum yield. *ACS Nano* 11, 10373–10383. <https://doi.org/10.1021/acsnano.7b05442>.
- Li, J., Xu, L., Wang, T., Song, J., Chen, J., Xue, J., Dong, Y., Cai, B., Sha, Q.N., Han, B., Zeng, H., 2017. 50-Fold EQE improvement up to 6.27% of solution-processed all-inorganic perovskite CsPbBr<sub>3</sub> QLEDs via surface ligand density control. *Adv. Mater.* 29, 1234. <https://doi.org/10.1002/adma.201603885>.
- Meysns, M., Perálvarez, M., Heuer-Jungemann, A., Hertog, W., Ibáñez, M., Nafria, R., Genc, A., Arbiol, J., Kovalenko, M.V., Carreras, J., Cabot, A., Kanaras, A.G., 2016. Polymer-enhanced stability of inorganic perovskite nanocrystals and their application in color conversion LEDs. *ACS Appl. Mater. Interfaces* 8, 19579–19586. <https://doi.org/10.1021/acsnano.6b02529>.
- Pan, A., He, B., Fan, X., Liu, Z., Urban, J.J., Alivisatos, A.P., He, L., 2018. Insight into the ligand-mediated synthesis of colloidal CsPbBr<sub>3</sub> nanocrystals: the role of organic acid, base and Cs precursors. *ACS Nano* 10, 7943–7954. <https://doi.org/10.1021/acsnano.6b03863>.
- Paul, T., Das, D., Das, B.K., Sarkar, S., Maiti, S., Chattopadhyay, K.K., 2019. CsPbBr<sub>2</sub>/g-C<sub>3</sub>N<sub>4</sub> Type II heterojunction as efficient visible range photocatalyst. *J. Hazard. Mater.* 380, 120855 <https://doi.org/10.1016/j.jhazmat.2019.120855>.
- Pu, Y.C., Fan, H.C., Liu, T.W., Chen, J.W., 2017. Methylamine lead bromide perovskite/protonated graphitic carbon nitride nanocomposites: interfacial charge carrier dynamics and photocatalysis. *J. Mater. Chem. A* 5, 25438–25444. <https://doi.org/10.1039/C7TA08190A>.
- Rao, L., Tang, Y., Yan, C., Li, J., Zhong, G., Tang, K., Yu, B., Li, Z., Zhang, J.Z., 2018. Tuning the emission spectrum of highly stable cesium lead halide perovskite nanocrystals through poly(lactic acid)-assisted anion-exchange reactions. *J. Mater. Chem. C* 6, 5375–5383. <https://doi.org/10.1039/C8TC00582F>.
- Roo, J.D., Ibáñez, M., Geiregat, P., Nedelcu, G., Walravens, W., Maes, J., Martins, J.C., Driessche, V., Kovalenko, M.V., Hens, Z., 2016. Highly dynamic ligand binding and light absorption coefficient of cesium lead bromide perovskite nanocrystals. *ACS Nano* 10, 2071–2081. <https://doi.org/10.1021/acsnano.5b06295>.
- Tang, Y., Cao, X., Honarfar, A., Abdellah, M., Chen, C., Avila, J., Asensio, M.C., Hammarström, L., Sa, J., Canton, S.E., Zheng, K., Pellerits, T., Chi, Q., 2018. Inorganic ions assisted anisotropic growth of CsPbCl<sub>3</sub> nanowires with surface passivation effect. *ACS Appl. Mater. Interfaces* 10, 29574–29582. <https://doi.org/10.1021/acsami.8b09113>.
- Wang, A., Guo, Y., Muhammad, F., Deng, Z., 2017. Controlled synthesis of lead-free cesium tin halide perovskite cubic nanocages with high stability. *Chem. Mater.* 29, 6493–6501. <https://doi.org/10.1021/acs.chemmater.7b02089>.
- Wang, H.C., Wang, W., Tang, A.C., Tsai, H.Y., Bao, Z., Ihara, T., Yarita, N., Tahara, H., Kanemitsu, Y., Chen, S., Liu, R.S., 2017. High-performance novel CsPbI<sub>3</sub>-xSnBr<sub>3</sub> perovskite quantum dots for highly-efficient light-emitting diodes. *Angew. Chem. Int. Ed.* 56, 13650–13654. <https://doi.org/10.1002/ange.201706860>.
- Wei, Y., Chen, Y., Cheng, Z., Lin, J., 2018. How to enhance the stability of lead halide perovskite quantum dots? *Sci. China Chem.* 48, 771–789. <https://doi.org/10.1360/N032018-00058>.
- Xie, J., Huang, Z., Wang, B., Chen, W., Lu, W., Song, J., 2019. A new lead-free perovskite Rb<sub>7</sub>Bi<sub>3</sub>Cl<sub>11</sub> nanocrystals with blue luminescence and excellent moisture-stability. *Nanoscale* 11, 6719–6726. <https://doi.org/10.1039/C9NR00600A>.
- Xu, H., Yuan, H., Duan, J., Zhao, Y., Jiao, Z., Tang, Q., 2018. Lead-free CH<sub>3</sub>NH<sub>3</sub>SnBr<sub>3-x</sub>I<sub>x</sub> perovskite quantum dots for mesoscopic solar cell applications. *Electrochim. Acta* 282, 807–812. <https://doi.org/10.1016/j.electacta.2018.05.143>.
- Yang, S., Chen, S., Mosconi, E., Fang, Y., Xiao, X., Wang, C., Zhou, Y., Yu, Z., Zhou, J., Gao, Y., Angelis, F., Huang, J., 2019. Stabilizing halide perovskite surfaces for solar cell operation with wide-bandgap lead oxysalts. *Science* 365, 473–478. <https://doi.org/10.1126/science.aax3294>.
- Yin, H.D., Wang, Q.B., Xue, S.C., 2004. Synthesis and structural characterization of diorganotin(IV) esters of salicylidene-amino acids. *J. Organomet. Chem.* 689, 2480–2485. <https://doi.org/10.1016/j.jorganchem.2004.05.004>.
- Zhang, M., Hua, Y., Miao, L., Qiong, W., Jung, Y., Lian, W., 2014. Composition-dependent photoluminescence intensity and prolonged recombination lifetime of perovskite CH<sub>3</sub>NH<sub>3</sub>PbBr<sub>3-x</sub>Cl<sub>x</sub> films. *Chem. Commun.* 50, 11727–11730. <https://doi.org/10.1039/c4cc04973j>.
- Zhang, X., Lin, H., Huang, H., Reckmeier, C., Zhang, Y., Choy, W.C., Rogach, A.L., 2016. Enhancing the brightness of cesium lead halide perovskite nanocrystal based green light-emitting devices through the interface engineering with perfluorinated ionomer. *Nano Lett.* 16, 1415–1420. <https://doi.org/10.1021/acs.nanolett.5b04959>.
- Zhang, M., Yu, H., Lyu, M., Wang, Q., Yun, J.H., Wang, L., 2014. Composition-dependent photoluminescence intensity and prolonged recombination lifetime of perovskite CH<sub>3</sub>NH<sub>3</sub>PbBr<sub>3-x</sub>Cl<sub>x</sub> films. *Chem. Commun.* 50, 11727–11730. <https://doi.org/10.1039/c4cc04973j>.